

Radiation and bias switch-induced charge dynamics in Al₂O₃-based metal-oxide-semiconductor structures

L. Sambuco Salomone, A. Kasulin, J. Lipovetzky, S. H. Carbonetto, M. A. Garcia-Inza, E. G. Redin, F. Berbeglia, F. Campabadal, and A. Faigón

Citation: *Journal of Applied Physics* **116**, 174506 (2014); doi: 10.1063/1.4900851

View online: <http://dx.doi.org/10.1063/1.4900851>

View Table of Contents: <http://scitation.aip.org/content/aip/journal/jap/116/17?ver=pdfcov>

Published by the [AIP Publishing](#)

Articles you may be interested in

[An investigation of capacitance-voltage hysteresis in metal/high-k/In_{0.53}Ga_{0.47}As metal-oxide-semiconductor capacitors](#)

J. Appl. Phys. **114**, 144105 (2013); 10.1063/1.4824066

[Charge trapping analysis of Al₂O₃ films deposited by atomic layer deposition using H₂O or O₃ as oxidant](#)

J. Vac. Sci. Technol. B **31**, 01A101 (2013); 10.1116/1.4766182

[Effect of annealing ambient and temperature on the electrical characteristics of atomic layer deposition Al₂O₃/In_{0.53}Ga_{0.47}As metal-oxide-semiconductor capacitors and MOSFETs](#)

J. Appl. Phys. **111**, 044105 (2012); 10.1063/1.3686628

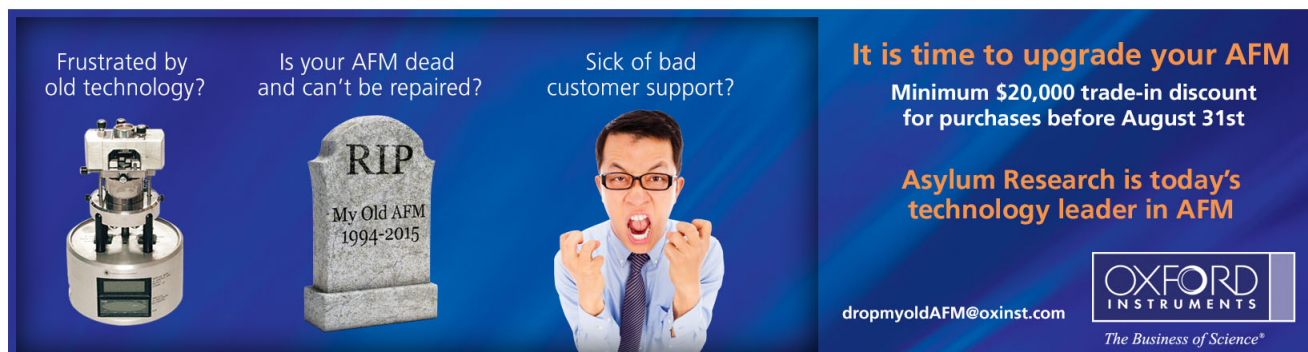
[Charge trapping characteristics of Au nanocrystals embedded in remote plasma atomic layer-deposited Al₂O₃ film as the tunnel and blocking oxides for nonvolatile memory applications](#)

J. Vac. Sci. Technol. A **30**, 01A104 (2012); 10.1116/1.3639131

[High density and program-erasable metal-insulator-silicon capacitor with a dielectric structure of SiO₂/HfO₂ – Al₂O₃ nanolaminate/Al₂O₃](#)

Appl. Phys. Lett. **88**, 042905 (2006); 10.1063/1.2168227

Frustrated by old technology? Is your AFM dead and can't be repaired? Sick of bad customer support?



It is time to upgrade your AFM
Minimum \$20,000 trade-in discount for purchases before August 31st

Asylum Research is today's technology leader in AFM

dropmyoldAFM@oxinst.com

OXFORD INSTRUMENTS
The Business of Science®

Radiation and bias switch-induced charge dynamics in Al₂O₃-based metal-oxide-semiconductor structures

L. Sambuco Salomone,^{1,a)} A. Kasulin,¹ J. Lipovetzky,^{1,2} S. H. Carbonetto,¹
 M. A. Garcia-Inza,¹ E. G. Redin,¹ F. Berbeglia,¹ F. Campabadal,³ and A. Faigón^{1,2}

¹Laboratorio de Física de Dispositivos—Microelectrónica, Instituto de Ciencias de la Ingeniería (INTECIN), Facultad de Ingeniería, Universidad de Buenos Aires, Av. Paseo Colón 850, C1063ACV, Buenos Aires, Argentina

²Consejo Nacional de Investigaciones Científicas y Técnicas (CONICET), Buenos Aires, Argentina

³Instituto de Microelectrónica de Barcelona (IMB)—Centro Nacional de Microelectrónica (CNM)—Consejo Superior de Investigaciones Científicas (CSIC), Barcelona, Spain

(Received 11 July 2014; accepted 21 October 2014; published online 5 November 2014)

Charge trapping dynamics induced by exposition to γ -ray (⁶⁰Co) radiation and bias switching in MOS capacitors with atomic layer deposited Al₂O₃ as insulating layer was studied. Electrical characterization prior to irradiation showed voltage instabilities due to electron tunneling between the substrate and preexisting defects inside the dielectric layer. Real-time capacitance-voltage (C-V) measurements during irradiation showed two distinct regimes: For short times, the response is strongly bias dependent and linear with log(t), consistent with electron trapping/detrapping; for long times, the voltage shift is dominated by the radiation-induced hole capture being always negative and linear with dose. A simple model that takes into account these two phenomena can successfully reproduce the observed results. © 2014 AIP Publishing LLC.

[<http://dx.doi.org/10.1063/1.4900851>]

I. INTRODUCTION

In recent years, Alumina (Al₂O₃) has become a promising material to be used as insulator in different applications in microelectronics. For example, it was proposed as a component of multilayer dielectric in ion-sensitive field effect transistors (ISFET).¹ It is also used as the interpoly dielectric/blocking layer in floating gate/charge trapping nonvolatile Flash memories yielding better coupling without reducing the physical thickness of the top dielectric.^{2–10}

Much effort has been devoted to the electrical characterization of Al₂O₃-based MOS devices,^{2–11} but little research was dedicated to the study of the radiation effects in these devices.^{12–16} In devices with a thin interfacial oxynitride layer, several interesting effects were reported

- (1) Xiong *et al.*¹² observed an increase of the low-frequency noise due to the increase of border traps density. A decrease of the low-frequency noise was observed after consecutive sessions of annealing at 200 °C during 24 and 48 h.
- (2) Felix *et al.*^{13,14} observed a maximum radiation-induced voltage shift at 1.0–1.3 MV/cm, similar to that observed in thermal oxides. They also observed a t_{ox}^4 dependence of the voltage shift on physical thickness, instead of the usual t_{ox}^2 . The authors explained this dependence as a result of charge removal by tunneling, which reduces the effective thickness of the dielectric. Finally, a decrease in the interface trap density with the applied dose was also reported in that work, presumably as a consequence of the passivation of interface states due to the hydrogen released during irradiation.

- (3) Zhou *et al.*¹⁵ studied the combination of irradiations and negative bias temperature stress (NBTS), showing that the oxide trap voltage shift (V_{ot}) after combined irradiation and NBTS was larger than the independent contributions added. This result was interpreted by the authors as the trapping of both positive and negative charges during irradiation, and the subsequent release of compensating electrons during NBTS. As regards the interface trap voltage shift (V_{it}), the combined irradiation with NBTS showed that both effects are independently added.

Related results combining radiation and electrical stress on SiO₂ can be found in Refs. 17–19.

Voltage instabilities in Al₂O₃-based devices under normal operating conditions were observed and identified as electron trapping/detrapping by tunneling transitions from/to the substrate.^{11,20–22} This voltage instability makes it difficult to characterize the radiation response, because it superimposes to the radiation effects, as described by Felix *et al.* for hafnium silicate (Hf_xO_ySi_z).²³ In a previous work, we characterized and modeled the electron traps that give place to these voltage instabilities.¹¹ The aim of this work is to analyze the γ -ray (⁶⁰Co) radiation response of Al₂O₃-based MOS capacitors under different bias conditions using a real-time measurement technique to discriminate the bias-induced electron trapping/detrapping and the radiation effects.

II. EXPERIMENTAL DETAILS

MOS capacitors with 11.7 nm Al₂O₃ grown by atomic layer deposition (ALD) as insulating layer were studied. The samples were fabricated on both an n-type phosphorus-doped silicon wafer with resistivity 1–12 Ωcm and on a p-type boron-doped silicon wafer with resistivity 4–40 Ωcm . The

^{a)}E-mail: lsambuco@fi.uba.ar.

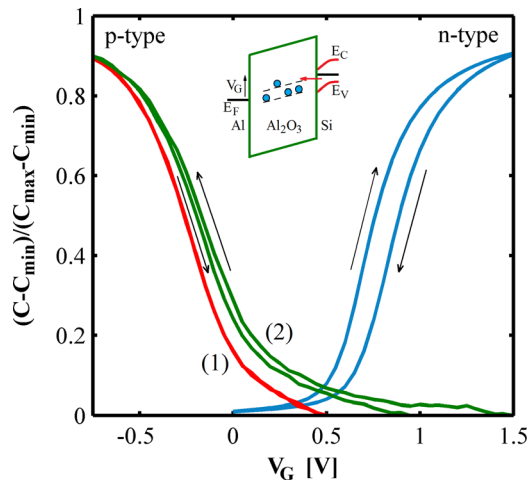


FIG. 1. Experimental C-V cycles for MOS capacitors with Al_2O_3 as insulating layer. The hysteresis expresses electron trapping in preexisting defects within the insulator by tunneling from the semiconductor as shown in the inset. Curve (1) in the p-type sample reaches a maximum voltage of 0.5 V and exhibits no hysteresis.

metallization was performed with $\text{Al}/(0.5\%)\text{Cu}$. The wafers underwent a forming gas ($\text{N}_2/(10\%)\text{H}_2$) annealing step at 350°C for 20 min. Transmission electron microscopy (TEM) images showed that the Al_2O_3 layer is amorphous, as expected for the low annealing temperature.²⁴ The estimated equivalent oxide thickness (EOT) yields a relative dielectric constant $\kappa = 7.4$.²⁵ A SiO_x interfacial layer (IL) was frequently reported as a sub-product of ALD layers growth on Si.^{7,26} We could not detect its presence through microscopy, neither through kinetics analysis. However, the low value of κ (7.4) compared with the reported amorphous Al_2O_3 κ -value (8.6),⁷ may be related to the possible presence of an IL in our samples. This issue was previously analyzed in detail in Ref. 11. More details about fabrication are given in Ref. 25.

The measuring system comprised a Boonton Electronics 72BD capacitance meter and a Burr-Brown UDAS-1000E data acquisition system (DAQ). The capacitance was measured at 1 MHz with a 15 mV RMS signal. During the measurement, the device under test (DUT) was biased with a constant gate voltage. Periodically, a C-V cycle from

inversion to accumulation and back to inversion was measured during ~ 2 s. The measurement was short enough to ensure that the change in gate bias does not affect the overall response to irradiation of the DUT.

III. RESULTS

A. Electrical characterization

An electrical characterization of the devices was performed before irradiation. Figure 1 shows C-V cycles for both capacitors (p-type and n-type substrates). A hysteresis phenomenon was observed in both n- and p-type capacitors when the gate voltage (V_G) reaches 1.5 V. However, for the p-type sample, the hysterical behavior can be avoided and the whole C-V curve measured (curve 1 in the figure), if V_G is lower than 0.5 V. This hysteresis is interpreted to be the result of trapping/detrapping along the C-V cycle of electrons tunneling from/to the semiconductor into preexisting defects within the insulator.^{11,20-22} These defects are more easily filled at higher V_G for this causes more oxide traps to lie below the Fermi level, as shown in the inset of Fig. 1.

The voltage needed to keep a constant capacitance (V_C) was tracked. The reference capacity was chosen at the high derivative part of the C-V curve. As was observed regarding the hysteresis, holding V_G at positive voltages causes electron trapping, shifting V_C . Therefore, the instability corresponding to the n-type sample is stronger than that for the p-type as shown in Fig. 2(a). Recently,¹¹ we characterized and modeled the time evolution of the voltage instability observed in n-type devices. This phenomenon makes it difficult to characterize the radiation response in real-time using n-type devices, because shifts in the C-V curves mask the radiation-induced charge trapping.

It is expected to observe the same behavior in p-type devices when the applied voltage is high enough. Fig. 2(b) confirms this hypothesis showing the shift in V_C after cumulative intervals of 15 min during which a constant voltage of 1 V was applied to the gate.

As a conclusion, for a first characterization of the radiation effects, the bias-induced voltage instability could be avoided if a p-type sample is irradiated with a low applied

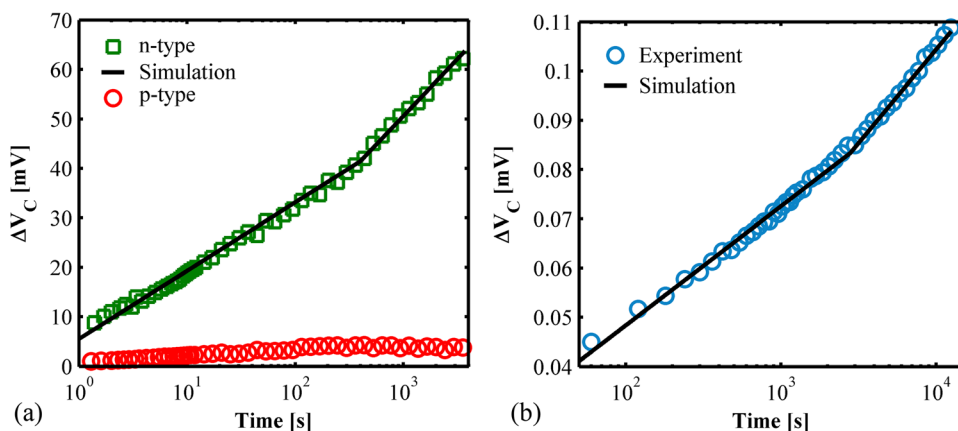


FIG. 2. (a) Experimental (symbols) and simulated (lines) V_C versus time curves for both types of substrates under constant capacitance measurements. Model parameters (n-type): $\alpha_1 = 6$ mV, $\tau_1 = 0.4$ s, $\alpha_2 = 4$ mV, and $\tau_2 = 400$ s. (b) Experimental (symbols) and simulated (lines) V_C versus time curve for the p-type capacitor stressed at $V_G = 1$ V. Model parameters: $\alpha_1 = 10.5$ mV, $\tau_1 = 1$ s, $\alpha_2 = 6$ mV, and $\tau_2 = 2800$ s.

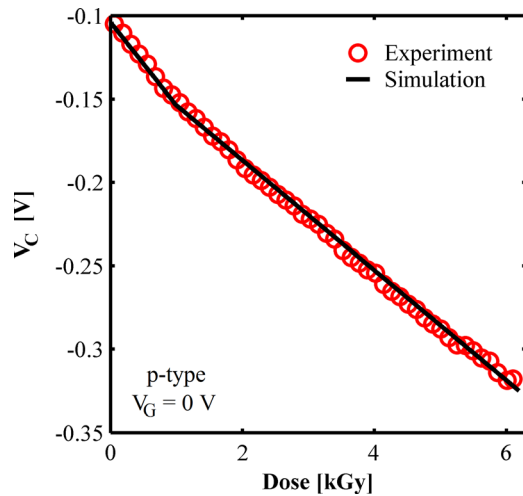


FIG. 3. Experimental (symbols) and simulated (line) V_C versus dose curve during the first irradiation session ($V_G = 0$ V). Model parameters: $\beta_1 = 50 \mu\text{V}/\text{Gy}$ ($D < 1$ kGy) and $\beta_2 = 33 \mu\text{V}/\text{Gy}$ ($D > 1$ kGy).

voltage, which prevents electron trapping. Once the main features of the radiation response are extracted from this experiment, measurements under different bias conditions could be performed to distinguish the bias-induced voltage instability and the radiation effects.

B. Radiation response

The Al_2O_3 -based p-type capacitor was exposed to different γ -ray (^{60}Co) radiation sessions with a dose rate of 23 ± 2 Gy/h. Doses are referred to SiO_2 . C-V curves were measured every 15 min in all sessions except for the first one, where the time between measurements was half an hour.

During the first session, the device was irradiated with zero bias up to a total dose of 6.2 kGy. A displacement with dose of the C-V curve towards negative voltages was observed, indicating an increase of positive trapped charge within the insulator. There is a linear dependence of V_C -shift with dose, as shown in Fig. 3, and no saturation of the positive charge buildup was observed in this experiment.

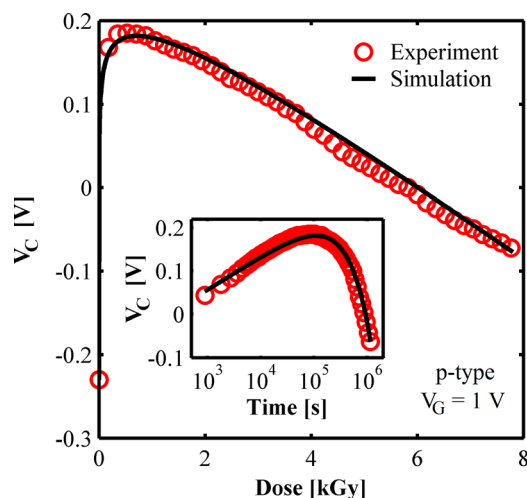


FIG. 4. Experimental (symbols) and simulated (lines) V_C versus dose curve during the second irradiation session ($V_G = 1$ V). Model parameters: $\alpha_1 = 34$ mV, $\tau_1 = 2000$ s, and $\beta = 48 \mu\text{V}/\text{Gy}$.

During the second session, the device was irradiated up to 7.8 kGy, with a constant applied voltage $V_G = 1$ V. Figure 4 shows the evolution of V_C with dose. A turn-around phenomenon was observed. For short times ($t < 10^5$ s, equivalent to 600 Gy), a positive V_C -shift is observed, whereas after 10^5 s, the V_C -shift changes and exhibits a negative slope. The response for $t > 10^5$ s is consistent with the capture of holes generated by radiation, as for the case of $V_G = 0$ V. In contrast, the initial positive V_C -shift was approximately linear with $\log(t)$ (see inset in Fig. 4), which is consistent with the electron capture by tunneling transitions from the substrate, as observed without radiation (Fig. 2). This superposition of both bias-induced electron trapping and radiation-induced hole trapping was also reported in HfO_2 .²⁷ A similar result was observed in LaAl_2O_3 and NdAl_2O_3 ,²⁸ although in these materials, both contributions (electron and hole trapping) seem to be related to the irradiation.

The post-irradiation response is shown in Fig. 5. The device was held with $V_G = 0$ V and C-V measurements were recorded every 15 min. The ΔV_C vs. time curve exhibits a negative shift linear with $\log(t)$, which was accelerated after approximately 10^4 s, still showing the $\log(t)$ dependence. This behavior is consistent with the results of voltage switching shown in Fig. 6 and is identified in Sec. IV as tunneling back of electrons trapped during the irradiation with positive gate bias. A similar result was observed in HfO_2 -based devices.²⁸

Afterward, the device was irradiated up to a total dose of 4.3 kGy with a biasing sequence $V_G = 1$ V \rightarrow 0 V \rightarrow -1 V. Figure 6 shows the results where the first stage ($V_G = 1$ V) has the already analyzed characteristics. After switching the gate bias ($V_G = 0$ V), V_C monotonically shifted to more negative voltages linear with $\log(t)$ for short times and linear with dose for long times. At short times after the switching, the electrons trapped during the first stage are detrapped by tunneling to the substrate. After approximately 5×10^4 s (~ 1.8 kGy), the radiation-induced hole trapping dominates the device response, changing the shape of the curve to the linear dependence with dose. Finally, switching

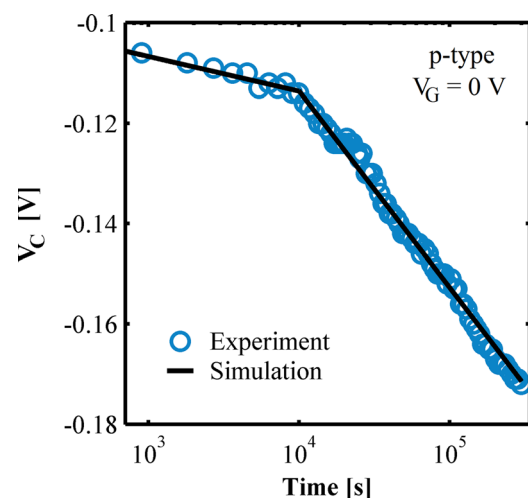


FIG. 5. Experimental (symbols) and simulated (lines) V_C versus time curve after the second irradiation session. $V_G = 0$ V between C-V measurements. Model parameters: $\alpha_1 = -3$ mV, $\tau_1 = 1$ s, $\alpha_2 = -14$ mV, and $\tau_2 = 10000$ s.

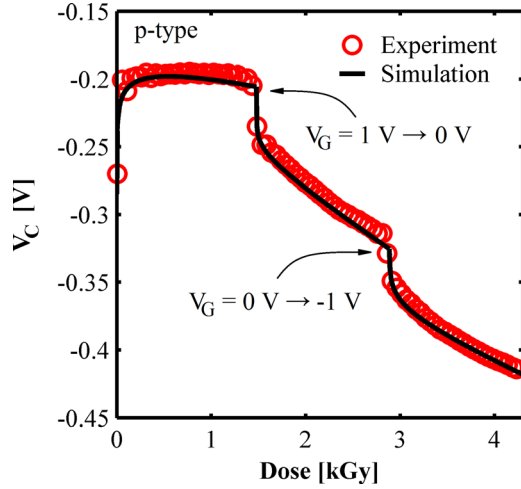


FIG. 6. Experimental (symbols) and simulated (lines) V_C versus dose curve during a switched bias irradiation. Model parameters: $\alpha = 11$ mV, $\tau = 13$ s, $\beta = 20$ μ V/Gy ($D < 1.5$ kGy), $\alpha = -5$ mV, $\tau = 3$ s, $\beta = 45$ μ V/Gy (1.5 kGy $< D < 2.9$ kGy), $\alpha = -7$ mV, $\tau = 150$ s, and $\beta = 29$ μ V/Gy ($D > 2.9$ kGy).

to a negative bias voltage ($V_G = -1$ V) favours the release of electrons captured at deeper energetic levels, while the radiation-induced hole capture continues.

IV. PHYSICAL MODEL

The voltage shift for a constant capacitance, $\Delta V_C(t)$, is related to the variation of the density of both tunnel-assisted trapped electrons and radiation-induced trapped holes

$$\Delta V_C(t) = \frac{q}{C_{ox}} \int_0^{t_{ox}} [\Delta n_t(x, t) - \Delta p_t(x, t)] \left(1 - \frac{x}{t_{ox}}\right) dx, \quad (1)$$

where q is the elementary charge, C_{ox} is the capacitance per unit area, t_{ox} is the Al_2O_3 thickness, Δn_t and Δp_t are the changes in the trapped electron and hole densities, respectively, and x is the position of the electron/hole traps from the substrate-insulator interface.

Tunneling transitions from/to the substrate causes a change in the density of trapped electrons¹¹

$$\frac{dn_t}{dt} = \frac{N_f f - n_t}{\tau}, \quad (2)$$

where N_t is the density of electron traps, f is the Fermi-Dirac occupation probability according to the Fermi level at the substrate, and τ is the tunneling time constant between electronic states in the substrate and the electron traps. A tunneling front approximation was considered.²⁹ Taking into account only, the electron traps contribution in Eq. (1)

$$\Delta V_C^{\text{tunneling}}(t) = \left(\frac{\hbar^2}{2m_{ox}}\right)^{1/2} \frac{qN_t\Delta f}{2C_{ox}\sqrt{E_t}} \ln\left(\frac{t}{\tau_i}\right), \quad (3)$$

where m_{ox} is the electron effective mass in Al_2O_3 , Δf is the change in the occupation probability due to the applied voltage, E_t is the trap energy level referred to the conduction

band edge, and τ_i is the tunneling time constant for the traps first reached by the tunneling front.

For radiation generated holes, the continuity equation is

$$\frac{dp_f}{dt} = -\frac{dj_p}{dx} + g_0 D_r Y - \sigma_p |j_p| (P_t - p_t), \quad (4)$$

where p_f is the density of free holes, j_p is the hole flux, g_0 is the generation of electron-hole pairs per unit dose, Y is the fractional yield, D_r is the dose rate, σ_p is the capture cross section, and P_t is the hole traps density. We assume that the hole traps are uniformly distributed across the Al_2O_3 layer.

For the dose rate used in this work, holes reach steady-state in a short time compared to the irradiation time,^{30,31} then $dp_f/dt = 0$. Moreover, taking into account, the observed linear dependence with dose of the hole capture contribution to the V_C -shift, we assume the low dose approximation $p_t \ll P_t$. Therefore, Eq. (4) can be integrated to obtain the hole flux as

$$j_p(x) = \frac{g_0 D_r Y}{\sigma_p P_t} [e^{-\sigma_p P_t (t_{ox} - x)} - 1], \quad (5)$$

The trapped holes density is given by

$$\frac{dp_t}{dt} = \sigma_p |j_p| P_t. \quad (6)$$

Replacing (5) in (6) and solving for p_t

$$p_t(x, t) = g_0 D(t) Y [1 - e^{-\sigma_p P_t (t_{ox} - x)}], \quad (7)$$

where $D(t) = D_r t$ is the total absorbed dose.

As for the case of electron traps, considering only the contribution of hole traps in Eq. (1)

$$\Delta V_C^{\text{radiation}}(t) = -\frac{qg_0 D(t) Y}{C_{ox}} \left[\frac{t_{ox}}{2} - \frac{1 - e^{-\sigma_p t_{ox} P_t}}{t_{ox} (\sigma_p P_t)^2} + \frac{e^{-\sigma_p t_{ox} P_t}}{\sigma_p P_t} \right]. \quad (8)$$

Taking into account both contributions, the fitting equation turns out to be

$$\Delta V_C(t) = \alpha \ln\left(\frac{t}{\tau_i}\right) - \beta D(t), \quad (9)$$

where α and β are related to physical parameters from (3) and (8).

V. CONCLUSIONS

The response of Al_2O_3 -based MOS devices under γ -ray (^{60}Co) irradiation and switched bias conditions was studied. The shifts with dose of the C-V characteristic represented by the evolution of the voltage corresponding to a chosen value of the device capacitance were tracked as a measure of the changes in the oxide charge.

The results can be described in terms of the superposition of two different trapping processes. One is related to tunneling transitions between substrate and electron traps near the $\text{Si}/\text{Al}_2\text{O}_3$ interface, strongly dependent on the bias condition. The second process is related to the trapping of

holes generated by the incident radiation. Due to the opposite charge trapped in each process, the evolution of the constant capacitance voltage (V_C) is non-monotonic. Electron trapping dominates the dynamic for short times until the hole capture contribution becomes more significant. The post-radiation measurements show the tunneling back of electrons trapped during the irradiation with positive gate bias. Considering the reported $\ln(t)$ dependence of the tunneling-assisted electron trapping/detrapping, and a linear dependence with dose for the radiation-induced hole capture, the experimental results were fairly reproduced by a simple model. This simplicity has to be complemented with detailed information on the electronic properties of the traps in order to have a real predictive model for different materials. The factor α involves the effective mass of the electrons in the material m_{ox} , the electron trap density N_t , and the traps energy E_t . Similarly, β embraces the generation factor g_0 , the generation yield Y , which, in turn, has a non trivial dependence on the electric field, density, and distribution of hole traps. Even though the complete required information is not generally available, the given expressions provide a tool for analysis and semi-quantitative predictions.

ACKNOWLEDGMENTS

This work had been supported in part by the University of Buenos Aires with Grant Y064, by the CONICET, by the ANPCyT PICT 2007-01907, by the INTECIN, and by the Spanish Ministry of Economy and Competitiveness through Project No. TEC2011-27292-C02-02. The authors would like to thank the Centro Atómico Ezeiza—Comisión Nacional de Energía Atómica, for the access to irradiation facilities, and Eva Pawlak, Elba Bof, and Brenda Redin Telles for their assistance with dosimetry.

¹H. J. Jang and W. J. Cho, *Appl. Phys. Lett.* **99**, 43703 (2011).

²D. Wellekens, P. Blomme, B. Govoreanu, J. D. Vos, L. Haspelslagh, J. Van Houdt, D. P. Brunco, and K. van der Zanden, in *Proceedings of the IEEE European Solid-State Device Research Conference* (2006), pp. 238–241.

³D. Shum, G. Jaschke, M. Canning, R. Kakoschke, R. Duschl, R. Sikorski, F. Erler, M. Stiftinger, A. Duch, J. R. Power, G. Tempel, R. Strenz, and R. Allinger, in *Proceedings of the IEEE Memory Workshop* (2009).

⁴R. Kakoschke, L. Pescini, J. R. Power, K. van der Zanden, E.-O. Andersen, Y. Gong, and R. Allinger, *Solid-State Electron.* **52**, 550–556 (2008).

⁵X. F. Zheng, W. D. Zhang, B. Govoreanu, D. Ruiz Aguado, J. F. Zhang, and J. Van Houdt, *IEEE Trans. Electron Devices* **57**(1), 288–296 (2010).

⁶C. H. Lee, K. I. Choi, M. K. Cho, Y. H. Song, K. C. Park, and K. Kim, *IEEE Int. Electron Devices Meet.* **2003**, 26.5.1–26.5.4.

⁷M. Specht, H. Reisinger, M. Städele, F. Hofmann, A. Gschwandtner, E. Landgraf, R. J. Luyken, T. Schulz, J. Hartwich, L. Dreeskomfeld, W. Rösner, J. Kretz, and L. Risch, in *Proceedings of the European Solid-State Device Research* (2003), pp. 155–158.

⁸L. Larcher, A. Padovani, V. della Marca, P. Pavan, and A. Bertacchini, in *Proceedings of the IEEE International Symposium on VLSI Technology, Systems and Applications (VLSI-TSA)* (2010), pp. 52–53.

⁹A. Padovani, L. Larcher, D. Heh, and G. Bersuker, *IEEE Electron Device Lett.* **30**(8), 882–884 (2009).

¹⁰A. Padovani, A. Arreghini, L. Vandelli, L. Larcher, G. Van den bosch, P. Pavan, and J. Van Houdt, *IEEE Trans. Electron Devices* **58**, 3147–3155 (2011).

¹¹L. S. Salomone, J. Lipovetzky, S. H. Carbonetto, M. A. García Inza, E. G. Redin, F. Campabadal, and A. Faigón, *J. Appl. Phys.* **113**, 074501 (2013).

¹²H. D. Xiong, D. M. Fleetwood, J. A. Felix, E. P. Gusev, and C. D'Emic, *Appl. Phys. Lett.* **83**, 5232 (2003).

¹³J. A. Felix, M. R. Shaneyfelt, D. M. Fleetwood, T. L. Meisenheimer, J. R. Schwank, R. D. Schrimpf, P. E. Dodd, E. P. Gusev, and C. D'Emic, *IEEE Trans. Nucl. Sci.* **50**(6), 1910–1918 (2003).

¹⁴J. A. Felix, J. R. Schwank, D. M. Fleetwood, M. R. Shaneyfelt, and E. P. Gusev, *Microelectron. Reliab.* **44**, 563–575 (2004).

¹⁵X. J. Zhou, D. M. Fleetwood, J. A. Felix, E. P. Gusev, and C. D'Emic, *IEEE Trans. Nucl. Sci.* **52**(6), 2231–2238 (2005).

¹⁶E. Yilmaz, I. Dogan, and R. Turan, *Nucl. Instrum. Methods Phys. Res., Sect. B* **266**, 4896–4898 (2008).

¹⁷D. M. Fleetwood, P. S. Winokur, and L. C. Riewe, *IEEE Trans. Nucl. Sci.* **37**(6), 1806–1817 (1990).

¹⁸D. M. Fleetwood, *IEEE Trans. Nucl. Sci.* **43**(3), 779–786 (1996).

¹⁹V. V. Emelianov, G. I. Zebrev, V. N. Ulimov, R. G. Useinov, V. V. Belyakov, and V. S. Pershenkov, *IEEE Trans. Nucl. Sci.* **43**(3), 805–809 (1996).

²⁰G. Puzzilli, B. Govoreanu, F. Irrera, M. Rosmeulen, and J. Van Houdt, *Microelectron. Reliab.* **47**, 508–512 (2007).

²¹W. D. Zhang, B. Govoreanu, X. F. Zheng, D. R. Aguado, M. Rosmeulen, P. Blomme, J. F. Zhang, and J. Van Houdt, *IEEE Electron Device Lett.* **29**(9), 1043–1046 (2008).

²²D. R. Aguado, B. Govoreanu, W. D. Zhang, M. Jurczak, K. De Meyer, and J. Van Houdt, *IEEE Trans. Electron Devices* **57**(10), 2726–2735 (2010).

²³J. A. Felix, D. M. Fleetwood, R. D. Schrimpf, J. G. Hong, G. Lucovsky, J. R. Schwank, and M. R. Shaneyfelt, *IEEE Trans. Nucl. Sci.* **49**(6), 3191–3196 (2002).

²⁴V. V. Afanas'ev, A. Stesmans, B. J. Mrstik, and C. Zhao, *Appl. Phys. Lett.* **81**, 1678–1680 (2002).

²⁵F. Campabadal, J. M. Raff, M. Zabala, O. Beldarrain, A. Faigón, H. Castán, A. Gómez, H. García, and S. Dueñas, *J. Vac. Sci. Technol. B* **29**, 01AA07 (2011).

²⁶G. D. Wilk, R. M. Wallace, and J. M. Anthony, *J. Appl. Phys.* **89**(10), 5243–5275 (2001).

²⁷S. K. Dixit, X. J. Zhou, R. D. Schrimpf, D. M. Fleetwood, S. T. Pantelides, R. Choi, G. Bersuker, and L. C. Feldman, *IEEE Trans. Nucl. Sci.* **54**(6), 1883–1890 (2007).

²⁸C. Z. Zhao, S. Taylor, M. Werner, P. R. Chalker, R. J. Potter, J. M. Gaskell, and A. C. Jones, *J. Vac. Sci. Technol. B* **27**(1), 411–415 (2009).

²⁹P. J. McWhorter, S. L. Miller, and W. M. Miller, *IEEE Trans. Nucl. Sci.* **37**(6), 1682–1689 (1990).

³⁰R. J. Krantz, L. W. Aukerman, and T. C. Zietlow, *IEEE Trans. Nucl. Sci.* **34**(6), 1196–1201 (1987).

³¹D.-S. Lee and C.-Y. Chan, *J. Appl. Phys.* **69**(10), 7134–7141 (1991).